Chapter

PVDF Based Flexible Ferroelectrics

Mudassar Shehzad, Liu Yang and Yaojin Wang

Abstract

The well-known ferroelectric polymer, Poly (vinylidene fluoride-trifluoroethylene) [P(VDF-TrFE)], has a larger polarization-electric field hysteresis loop and possesses a high degree of crystallinity than poly(vinylidene fluoride-trifluoroethylene-clorotrifluoroethylene) [P(VDF-TrFE-CTFE)]. [P(VDF-TrFE-CTFE)] is a relaxer that contains its third monomer, CTFE, and breaks the coherence of its polarization domains in a nano polar region. It eventually shows narrower polarization PE loop characteristics than a normal ferroelectric polymer. The blended solution was dispensed in freestanding films and its beta phase enhancement was further studied which may have an impact on its electroactive characteristics. The electroactive properties, especially pyroelectric (PyE), piezoelectric (PE), and flexoelectric (FLE) properties of the blends are associated with its beta phase characteristics. Flexible electronics benefit greatly from the use of electroactive devices; however, a significant drawback of this technology is its higher power consumption combined with somewhat lower efficiency. To address this issue, we fabricated thin film devices designed to transmit and record electrical signals for pyroelectric and piezoelectric transduction within a single unit. These devices were constructed using a straightforward technique that involved creating sandwiched layered structures with a small radius. Ultimately, the printed thin film devices, which contained the enhanced ß phase, functioned effectively as both pyroelectric energy harvesters and piezoelectric transducers, among other applications.

Keywords: Olsen cycle, ferroelectric polymer, energy harvesting, electrostriction, polarization, antiferroelectric (AFE) loop, energy density, piezoelectric properties, sound pressure level, sound intensity, and piezoelectric transducers

1. Introduction

Polyvinylidene fluoride (PVDF) is recognized as an electroactive polymer that is used in both industrial and medical purposes. However, its widespread adoption is hindered by its lower density and reduced electric strain capabilities. A major challenge in utilizing these polymers is finding ways to decrease their high-power density through various technological approaches. For instance, in 2011, researchers led by Zhang discovered a method to enhance the electrostrictive performance of copolymers and terpolymers, which allows for greater energy density in PVDF. Nevertheless, this advancement involves intricate synthesis techniques and complex polymerization

processes [1]. Recently, P(VDF-TrFE) copolymer has shown a high electric polarization and electromechanical (EM) response compared to other established ferroelectric materials [2]. Researchers are currently concentrating on PVDF-based copolymers and terpolymers due to their remarkable ferroelectric characteristics. The copolymer shows substantial electric strain when subjected to high-energy electron irradiation of the films. These irradiated films display high energy density, making them highly appealing for a variety of electromechanical applications [3–5]. **Figure 1** illustrates three configurations of polymer chains: 'trans-gauche-trans-gauche' (TG + TG-), all 'trans' (TTT), and long trans 'TTTG+TTTG-'.

In the polar region of P(VDF), the packing morphology contributes to the enhancement of its polarization. The α phase, typically associated with TG+ and TG- conformations, lacks polarization due to the antiparallel alignment of the polymer chains in this amorphous form. In contrast, the β phase, where two all-trans chains are oriented parallel to each other, is crystalline and exhibits highly notable electrical properties due to its substantial dipole moment within each unit cell. The polar γ phase is characterized by alternate TTTG+ and TTTG- conformations, with dipole moments aligned in the same direction. After irradiation, PVDF polymers are converted into relaxor ferroelectrics, achieving high dielectric and polarization constants. Introducing structural defects is the primary mechanism by which conventional ferroelectrics are transformed into relaxor ferroelectric chains. Furthermore, relaxor

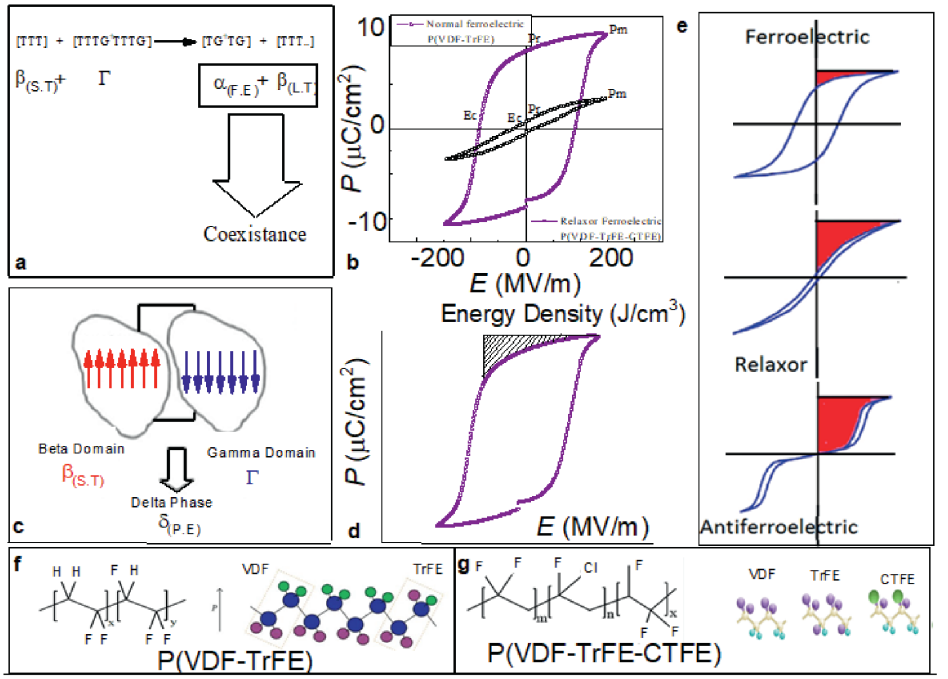

Figure 1.
AFE property of polymer. (a) The three (3) conformations such as long (trans) and short (trans) and trans gauche are responsible for the ferroelectric behavior, where α phase is regarded as the Ferroic Alpha phase. (b) Shows the conversion of co to the terpolymer after complete incorporation of (CTFE) into the PVDF-TrFE copolymer. (c) Shows an interaction among ß and Γ phases which results delta phase. (d) Shows the measurement of energy density (stored). (e) The graphical representation of ferroelectric (FE), Releaxor Ferroelectric (RFE) and Antiferroelectric (AFE) hysteresis loops. (f, g) The molecular chains of PVDF-TrFE and P(VDF-TrFE-CTFE) polymers.

ferroelectric properties can also be attained by substituting a third CTFE monomer within the polymer chain.

Antiferroelectric (AFE) behavior is distinguished by double hysteresis loops (DHL), which feature a central notch. This distinctive, propeller-shaped double hysteresis loop is a unique characteristic of AFE polymers, contributing to their high dielectric constants and substantial energy density. Among the different phases, the β phase stands out as the most important, as it offers strong crystalline properties essential for AFE double hysteresis loop behavior. Traditional ferroelectric materials have the lowest energy density, exhibiting broad polarization, whereas ferroelectric polymers generally achieve high maximum polarization (Pm) and low remnant polarization (Pr). Polymers can be classified into ferroelectric, paraelectric (PE), and antiferroelectric (AFE) types. Paraelectric and antiferroelectric polymers, often referred to as linear materials, have tunable polarization that varies with the applied electric field. For linear materials, energy density is directly proportional to the square of the electric field [6].

Upon applying an electric field, the dipoles align with the direction of the applied field (E). Notably, in materials with a high-energy dielectric density, the dipole orientation (DO) shifts, causing the electric field to either become trapped or released. Antiferroelectric polymers, with an almost zero net dipole moment, are the only means of generating stored electricity in this way. Thus, the antiferroelectric-like (AFE) behavior of the displacement electric (DE) field loop is essential, as it ensures full energy release during electric field conversion. The charged and discharged energy densities are assessed from the DE loop, and calculated by approximating the area under the shaded region in the DE hysteresis loop. The unreleased (or undischarged) energy density is defined as $U_{undischarge} = 100^{*}(1\text{-}U_{released}/U_{stored})$, where U_{stored} has the same value as $U_{unreleased}$ [6].

Flexible piezoelectric materials are recognized to change mechanical energy into electrical energy (direct piezoelectric materials). It can also change the electrical energy to mechanical energy (inverse piezoelectric materials) [1–3]. The inverse and direct piezoelectric materials can detect and transmit electric signals proficiently. For the flexible electronic devices and those having complex forms and manuring may need novel materials that can be stretchy and flexible to perform the essential work. In this persistence, a piezoelectric coefficient plays a huge role in choosing the right material, such as, the piezoelectric coefficient of ferroelectric ceramics and single crystals is in order of 1000 and 4000 pC/N respectively [4, 5]. The piezoelectric coefficient of PVDF polymers is much smaller than that of piezoelectric ceramics [7]. The main disadvantage of perovskite ceramics is that they are massive, heavyweight, and stiff, and cannot be fit to use in a flexible and wearable device. The stiffened nature of these ceramics makes it inappropriate to use them in various applications. To improve the piezoelectric features of polar polymer, the polymer composites can be used that can enhance the piezoelectric coefficient and preserve its elasticity too [8–14]. The incompatible electrical and mechanical features are a key task when adding any kind of ceramic filler to the polar polymer matrix. It may delay the performance of the stretchy piezoelectric polymer composites. The mismatch in dielectric permittivity between ceramic and polymer introduces a discontinuity in electric polarization at the matrix-filler interface, potentially forming an electric double layer that impedes the dielectric response of ceramic fillers. This disparity in permittivity across the matrix and filler can result in polarization loss, ultimately affecting performance. Various methods are being employed to establish conductive pathways for both electric polarization and mechanical load within the polymer matrix to enhance the strength of polymer composites. For instance, polymers are reinforced in three dimensions using a

low magnetic field [15], using freezing of ice to build complex composites [16], or bio-inspired assembly of nanoplatelets in a polymer matrix [17, 18]. However, these strategies generally result in a high-volume fraction of ceramic fillers, significantly compromising the mechanical flexibility of ceramic-polymer composites [6, 8, 19–21].

The key objective of our research work is to produce and select the right piezoelectric material for flexible acoustic devices like microphones and magnet-free loudspeakers. Since realizing the piezoelectric features of PVDF-based polymers, scientists have been looking for ways to fit in transparent piezoelectric devices into today's rapidly developing smart device ethos [21]. PVDF polymers are lighter in weight, transparent, and can be processed by using simple techniques [22–25]. PVDF polymers have good ferroelectric, pyroelectric, piezoelectric, and flexoelectric properties, making them perfect for transparent actuators and sensors. Investigators also tried to study the electroacoustic (EA) features of polymers. One such application that utilizes its inverse piezoelectric effect is the transparent thin film loudspeaker. Unlike traditional magnetic speakers, thin film loudspeakers operate primarily at a higher voltage. The high operating voltages of such piezoelectric materials limit their widespread use in many current technologies such as low-power mobile screens or smartphones etc. However, traditional speakers also have great limitations in their applications such as heavy and their reliability on electrical coils.

The main characteristic of ferroelectric polymers is the presence of switchable polarization and its domain boundary structure. Ferroelectric and resistive memory, electromechanical, and transport features are related to polarization switching behavior [26]. PVDF-based ferroelectric polymers have fantastic energy harvesting, electrostatic, and conductivity and excellent sensing properties in comparison to other ferroelectric polymers [27, 28]. Recent studies have shown that ferroelectric blends are able to control the structural properties of these materials and have good results in increasing phase percentage [29]. Gomes et al. stated that the degree of stretch and temperature greatly influences the transition from the non-polar alpha phase to the polar beta phase in PVDF-based polymers. Recently, Alexander De. Neef et al. studied that PVDF mixed with PMMA [30] has a piezoelectric coefficient (d_{33}) of up to 11 pCN^{-1}. Therefore, by poling the PVDF blends, the beta phase percentage, piezoelectric properties, and electrochemical properties can be improved. Chen et al. studied the acoustic properties of P (VDF-TrFE) and P (VDF-TrFE-CTFE) compounds by blending precise amount of copolymer in the beta phase of terpolymers [31]. The non-polar alpha phase progresses gradually and slowly to the polar beta phase. The copolymer is mixed in proportion to the terpolymer which enhances the beta phase reflection because of electrical and thermal poling.

Here we propose that we can enhance the pyroelectric, piezoelectric, and flexoelectric coefficients of the blends. The novel fabrication technique is adopted to enhance the electroactive properties of the polymer blends. It will also enhance the piezoelectric and flexoelectric coefficient with the improvement in stiffness and by imparting the stretchability in the blend matrix. The chain structure of the corresponding polymer phase is given in **Table 1**.

1.1 Material preparation

Copolymer, P(VDF-TrFE) 70/30 mole% is normal FE, and terpolymer, P(VDF-TrFE-CTFE) 70/20/10 mole% is a Relaxor FE. These polymers are subjected to characterization for their inherent properties, after mixing with each other in a definite proportion. Terpolymer and copolymer were dissolved in methyl isobutyl ketone (MIBK) separately

Phases	Dipole alignment	Polarization	Comments	Chain Structure
Alpha (α)	↑↓	✗	TG^+, TG^-	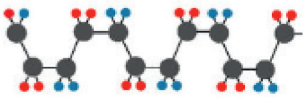
Beta (ß)	↑↑	✓	TTTT	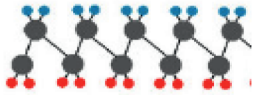
Gamma (Γ)	↓↓	✓	$TTTG^+$, $TTTG^-$	
Delta (δ)	↑↓	✗	Paraelectric Phase	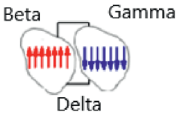
• Hydrogen • Fluorine ● Carbon				

Table 1.
Phases and their polarization responses based on literature review [32].

and mixed with each other in a definite stoichiometric ratio. Blend solution of 10% of P(VDF-TrFE) and 90% of P(VDF-TrFE-CTFE) is called here as α = 1 where α is copolymer content in a definite proportion of terpolymer solution. Also, α = 0 is 0% copolymer in 100% terpolymer, 0.1 is 10% copolymer in 90% of terpolymer solution, and so on. The film was fabricated using blends ranging from α = 0 to 1. Consequently, the films thickness ca. 20 to 30 microns were fabricated by the hand and machine layup method by adopting the solution cast method. The blend is dispensed at the glass plate to fabricate the thin films, and these films were cast by the machine-layup method to maintain its smoothness. Additionally, the cast films were annealed in heating furnaces to improve their crystalline properties. We have also observed that the annealing temperature governs as a key factor in predicting various properties of the above solution 0 < =α < =1.

2. Energy harvesting for flexible electronics

2.1 Pyroelectric energy harvesting (PyEH)

Energy storage is needed in the modern era, especially after the industrial revolution in this world. Scientists are trying to construct self-powered and independent devices with less power consumption. The demand for these devices is growing day after day in electronics industries [33]. Consequently, scavenging methods are developed by scientists in these methods wasteful energy is stored [34–37]. The major types of scavenging energy harvesting techniques include wasteful energy harvesting from mechanical energy by using the piezoelectric

properties, thermal energy harvesting through the Olsen power cycle using the pyroelectric effect [38], magnetic energy harvesting and photoelectric energy harvesting through solar cells [39].

Figure 2 represents the schematics of ferroelectric polymer heating at high temperature, because of the Olsen power cycle that ultimately harvests the energy due to the additional polarization by charge buildup at electrodes by reducing the temperature. It also indicates the alignment of domains upon heating the pyroelectric material up to the ferroelectric to paraelectric phase transition temperature.

In Pyroelectric energy harvesting, the wasteful heat is difficult to capture and labeled as a low-grade waste product [41]. To capture the wasteful scavenging heat energy, thermoelectric and/or pyroelectric energy harvesting practices can be used. If the antiferroelectric energy harvesting is carried out at ambient temperature; the technique is defined as room temperature energy harvesting technique, while if the energy storage takes place by tuning the temperature of antiferroelectric polymers; referred to as pyroelectric energy harvesting [42]. The pyroelectric material uses the wasteful heat energy and converts it to the electrical energy using the temporal temperature gradient [43, 44].

The antiferroelectric polymers store the room temperature electrical energy if these are made up as capacitors [45]. Instead, the pyroelectric polymers are used as a thermal sensing device. If the energy storage capacity of these materials is high enough to charge the low voltage electronic devices, then these materials can be used as pyroelectric energy harvesters shown in **Figure 3**. Since the 1960s the discovery of the pyroelectric effect, it is still considered as a less studied area [46–48].

2.2 Wasteful heat energy harvesting

Interestingly, the high ECE of antiferroelectric materials has attracted great interest due to their superior cooling efficiency compared to conventional methods such as gas evaporation [49, 50]. ECE is the adiabatic temperature difference of a dielectric material as a result of the dipolar effect generated during the action of an

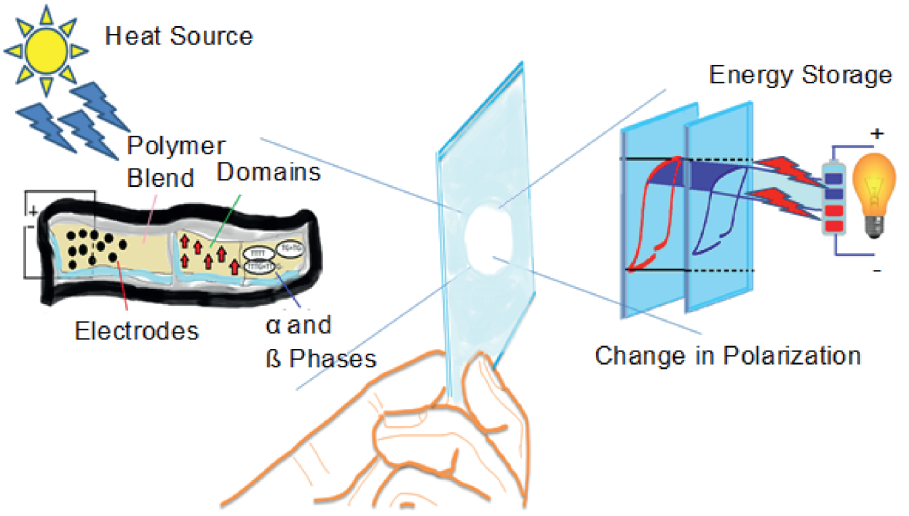

Figure 2.
Schematics of ferroelectric polymer heating at high temperature (i.e., 25°C < T < Tc) where Tc is the curie temperature [40].

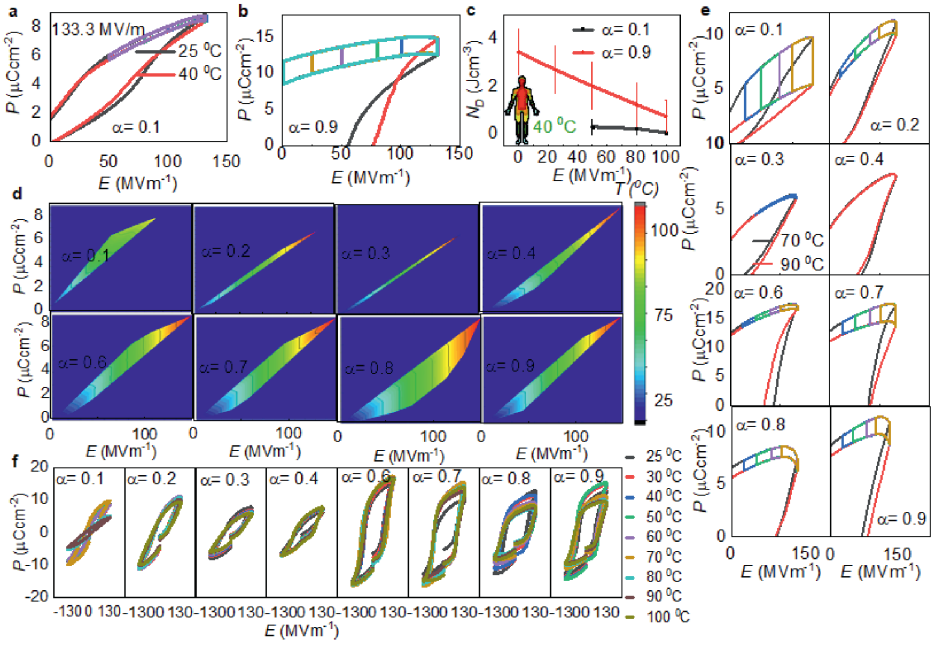

Figure 3.
The pyroelectric energy harvesting (PyEH) near a body temperature at T_1 = 25°C (77°F) and T_2 = 40°C (104°F) at E_H = 133 MV/m at 100 Hetrz frequency. (a) α = 0.1, (b) α = 0.9, and (c) shows the comparison of energy density (N_D) for α = 0.1 and 0.9 blends. (d) Shows the polarization-electric field and temperature contour graph for α =0.1, 0.2, 0.3, 0.4, … 0.9 blends. (e) Shows Olsen power cycle for α = 0.1 to α = 0.9 blends EL = 0 MV/m EH = 133.33 MV/m from 70 to 90°C at 100 Hz. (f) The temperature-dependent P-E hysteresis loop at E = 133.33 MV/m at 100 Hz frequency of α = 0.1 to 0.9 blends. (Standard deviation: n = 8) [40].

electric field [51]. It is well-known that the dipoles of a dielectric material follow an alignment path applied to an electric field. Changing the direction of the electric field will then reverse the orientation of this dipole [10]. The variation of the direction of the electric field causes a certain degree of randomness, also called the entropy of the system. Such an ordered dipole scheme leads to smoother effects of the dielectric material. Various types of materials have been reported to exhibit ECE effects, such as Polyvinylidene difluoride (PVDF) and so on.

Ferroelectric polymers gained the remarkable consideration of scientists' community because of their valuable large ECE [10, 51], enhanced dielectric constants [52, 53], improved electric properties (i.e., energy density), and remarkably improved electro-mechanical-actuation [54]. Electrocaloric effects can also be attributed to heat transfer from the PVDF samples to the ferroelectric heat source and to the paraelectric heat transfer coefficient. The δ-phase paraelectric phase at high temperatures, while the ß-phase plays a role in the crystallization phase of the material at high temperatures, which is due to the presence of the bulk TrFE group in the bulk chain of the PVDF-based polymer [5]. Here, the Beta (ß) phase is under consideration where it experiences a phase transition between the normal FE phase and the piezoelectric (PE) phase [14]. **Figure 4** shows the adiabatic temperature difference, which depends on the frequency acting on the constant electric field (E (MV/m)). In the ß phase, the polymer chains are usually aligned in the TTTT configuration, and the chain alignment is dependent on the dipole orientation. The temperature changes are responsible for the phase changes of all transitions to TG, such as TGTG′ and TTTG′ [3].

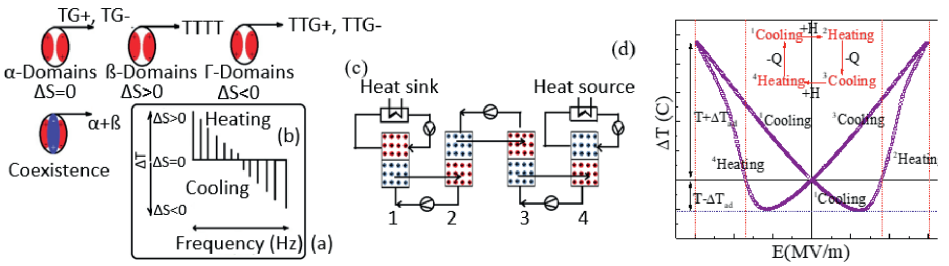

Figure 4.
Schematics of dipolar array. (a) shows randomness degree which helps to change its phase from TTTT to TGTG'. More randomness will be achieved if reduce the frequency, (b) gives the information of variation in adiabatic temperature (ΔT_{ad}) with decrease in frequency, (c) represents the illustration of heating cycle of a FE based Olsen heat engine and (d) shows the ΔTE loop [55].

The change in temperature (variation in adiabatic temperature) addressed and reported as 10°C when electric field is reduced to zero [3]. According to the ECE Landau–Devonshire theory, the entropy change in the isotherm is directly proportional to the square of the electrical conductivity with respect to ΔD.

$$\left[\Delta S = \frac{-1}{2}\beta_{LD}\Delta D^2\right] \tag{1}$$

where, $ß_{LD}$ is the term used for Landau-Devonshire coefficient from his theory [15].

P(VDF-TrFE-CTFE) and P(VDF-TrFE) are two types of polymers that have been extensively studied due to their ECE effects. The electric field in a dielectric material is defined as $D = E_0E + P$, where D is the electrical conductivity of the material, P is the polarization ($\mu C/m^2$) and E_0 is the free space permittivity. It is generally agreed that there are two types of dielectric polymers, linear and nonlinear polymers. In polymers, P_0 increases the strength of the electric field called linear material. During the phase change from ferroelectric to paraelectric, the temperature gradient at the Curie temperature (Tc) is determined by the thermal conductivity of the material. Various scientific publications have well-documented the differences between P(VDF-TrFE) and P(VDF-TrFE-CTFE) as secondary to F-P (ferroelectric paraelectric) is the polarization-dependent free energy of the polymer second-order phase transition, and it can be written in Eq. 2,

$$G = G_0 + \frac{1}{2}\beta_{LD}\left(T - T_c\right)P^2 + \frac{1}{4}\xi P^4 - EP \tag{2}$$

Eq. 2 β_{LD} can be reached, where T is the temperature determined by the DE path temperature (298.15) K, Tc = Currie temperature (°C or K), $\mathcal{E} = \mathcal{E}_0\mathcal{E}_r$ = dielectric permittivity, C/Vm, Polarization = (C/m^2) and E = electric field (10^6 V/m). The adiabatic change in temperature (ΔT) and entropy change (ΔS) are directly related to mechanical stress and strain, the rate is always linear.

$$\Delta T = \frac{-1}{2C_E}\beta_{LD}TD^2 = \frac{T\Delta S}{C_E} \tag{3}$$

ΔS (Joule/Kg*K), which represents the response to entropy change, and ΔT (°C) represents the adiabatic temperature response due to dipole disorientation. Cp is

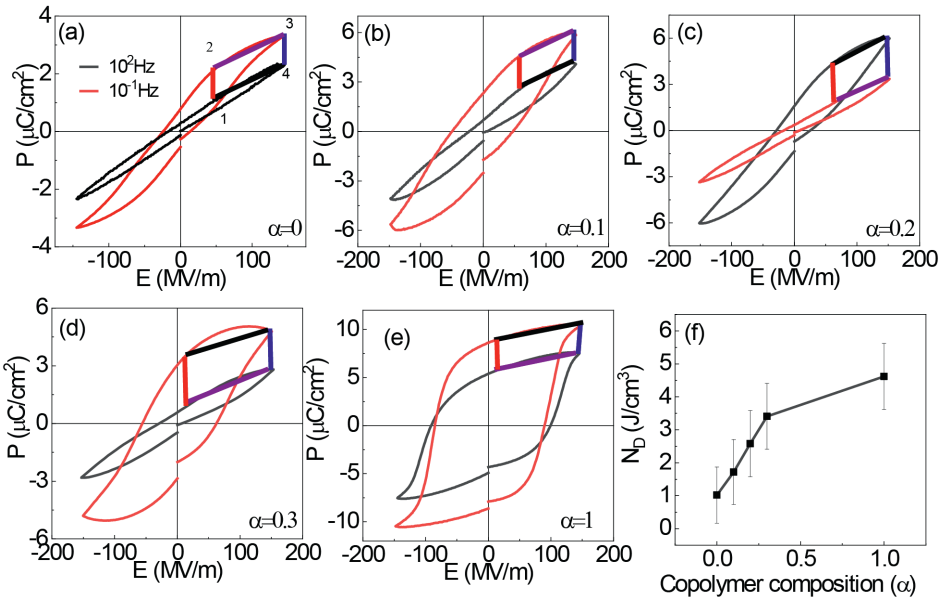

Figure 5.
Frequency dependent Olsen power cycle. a–e The Olsen power cycle of blends at 10^2 and 10^{-2} Hz. f Energy density comparison of polymer blends depending on the copolymer contents [55].

the specific heat capacity, β is the thermal conductivity ((Joule*m)/(K*C^2)), and C_E (Joule/Kg*K) is the thermal conductivity of the material used in the DSC values. More specifically, the specific heat capacity Cp (Joule/K) is expressed as,

$$\frac{dH}{dt} = C_P \frac{dT}{dt} + f(t,T) \tag{4}$$

Here, dH/dT = Heat Flow Signal (mWatt), dT/dt = Heating rate (10°C/min)) and m = mass (mg). The change in the enthalpy (ΔH) measured by area under the curve i.e.

$$\Delta H = \int_{T_1}^{T_2} C_E dT = \frac{Joule}{Kg*K} * K = \frac{Joule}{Kg} or \frac{Joule}{g} \tag{5}$$

Figure 5 shows the voltage-dependent Olsen force cycle. **Figure 5(a–e)** shows the integrated Olsen power cycles at 10^2 and 10^{-2} Hz. **Figure 5(f)** shows the energy balance of the polymer blends based on the copolymer core.

The ferroelectric properties, dielectric properties and electrocaloric susceptibility of P(VDF-TrFE), P(VDF-TrFE-CTFE) were investigated herein. Using mixing concentrations, the field and frequency dependence of ECE on blends are investigated.

3. Flexible and transparent piezoelectric transducers

3.1 Flexible and transparent piezoelectric loudspeaker

These days the need for lightweight and thin piezoelectric loudspeakers is rising for mobile phones and other touchscreen applications. Nowadays, researchers

are fabricating low-powered thin, and transparent loudspeakers. Various types of loudspeakers exist such as coil loudspeakers, electrostatic loudspeakers, piezoelectric loudspeakers, etc. The high-quality reproduction of sound is obtained by the traditional coil loudspeakers with permanent magnets to generate sounds [56].

These coil loudspeakers are bigger in volume and heavier in weight therefore cannot be used in smart devices [57]. While the electrostatic loudspeaker (ESL) uses the electrostatic field-activated thin diaphragm with low distortion it lacks the base response during its performance [58].

The piezoelectric loudspeakers were announced to overcome the disadvantages of coil and ESL loudspeakers [59]. It can overcome the high voltage problem of ESL because it uses an electric field to convert it into sound without using any magnetic coil. The piezoelectric loudspeakers use the electric field to produce the sound by altering its dimensions in response to the input signals. The mechanical actuation of the diaphragm ultimately alters its electric field into the sound. The frequency response in piezoelectric loudspeakers is limited and needs to be enhanced. If it is improved then it can transform the touch screen industry due to its exclusive feature of miniaturization, flexibility, and quick response for the loudspeaker business. The rewards of piezoelectric loudspeakers cover better transient response without moving coil, lower damping loss, no interference of external magnetic field, high impedance and low harmonic distortion etc. [60]. **Figure 6** represents the schematics of transparent and flexible piezoelectric loudspeakers created by electroactive polymer blends.

In 2003 Li et al. proposed the flexible loudspeaker which has the sound pressure level 80 dBSPL [62]. But in 2009 Sugimoto et al. presented his PVDF-based flexible and transparent loudspeaker with better performance [63]. In this research, we have proposed a loudspeaker with 91 dBSPL and better noise reduction characteristics. We have reported that the transduction property of piezoelectric loudspeakers is directly linked with their beta phase characteristics shown in **Figure 7**. Similarly, we have developed the flexoelectric microphone based on the flexoelectric effect discussed in Section 3.2 in detail. The high sensitivity is attained due to the zeta phase which is due to the reaction between α and ß phases shown in FTIR spectra.

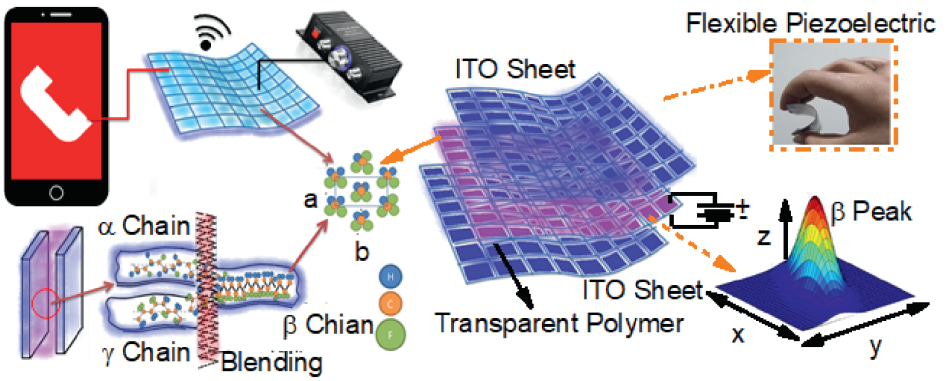

Figure 6.
The schematics of a flexible, transparent, and durable piezoelectric speaker, which is fabricated by wrapping the polymers between a pair of two (2) indium-titanium oxide electrodes. The schematics also represent the ß chain structure of copolymer which is fabricated in the result of the reaction between their α and Γ phases during blending [61].

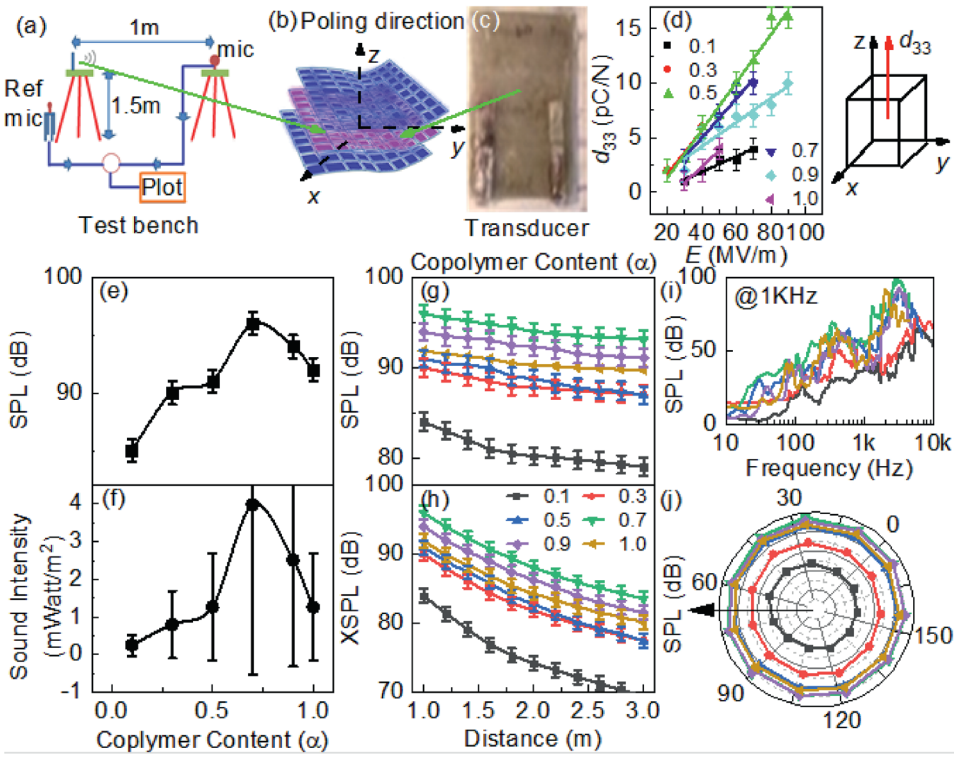

Figure 7.
Shows the transduction and piezoelectric properties of polymer speakers. (a) The schematic diagram of the test configuration for measurement of acoustic properties according to ISO standard. (b) Shows the poling direction (c) Picture of an actual device. (d) d_{33} of blends. (e) Sound Pressure Level graph at one meter away from the target at c.a 10^2 Vpp. (f) Describes the SI (i.e., W/m^2) plot at one meter away from the target at 10^2 Vpp (approx.). (g) Shows the SPL Vs distance from the target (m) graph. (h) The inverse graph at various distances (m). (i) Gives the information on sound pressure level vs. frequency at 1 kilohertz. (j) Shows the color-polar trend of sound pressure level at 1 kilohertz. (Standard deviation: n = 6) [61].

3.2 Flexible and transparent flexoelectric microphone

The polarization behavior of PVDF-based polymers is influenced by their polar and non-polar phases, specifically their flexoelectric properties. A critical factor in enhancing polarization is the packing morphology of the polar β-phase. Fourier transform infrared spectroscopy analysis aids in elucidating the trans gauche' configuration, commonly referred to as the α (amorphous) phase. In this α phase, the polymer chains are packed in an antiparallel manner, resulting in a lack of polarization or polarity. Conversely, in the ß phase, the two TTTT domain configurations align in parallel orientations, contributing to the material's polarization capabilities [8]. The electrical properties of the beta phase (crystal) are particularly intriguing, primarily due to the inherent dipole moment found in its lattice cell. In the polar gamma phase, dipole moments are aligned in the same direction, resulting from the alternating conformations of TTTG+TTTG−. Following irradiation, PVDF-based polymers can be converted into relaxor ferroelectrics, which exhibit large polarization and high dielectric constants. This transformation from standard ferroelectrics to relaxed ferroelectric chains is mainly driven by the formation of structural defects. Additionally, incorporating a different CTFE monomer in the polymer chain can also lead to the development of relaxor ferroelectric properties [20, 21].

This study involved the integration of a standard ferroelectric with a relaxor ferroelectric, which enabled us to observe a seamless transition between polar and non-polar phases. Consequently, drawing from the previous literature, we believe that the reflection peak in the FTIR spectrum contributes to the enhanced FE and flexoelectric (FLE) characteristics of the blend system which appears at 1337 cm^{-1} of FTIR spectra (see **Table 2**). In our previous research, we fabricated transparent and flexible piezo-speaker (TFPS) [22]. In this study, we fabricated a transparent and flexible flexo-microphone (TFFM) made of a P(VDF-TrFE) blend, as shown in **Figure 8**. **Figure 8(a)** The schematic illustrates a TFFM integrated into a smartphone screen. The transparent microphone utilizes flexoelectric properties to facilitate the conversion of acoustic signals into electrical signals. This process generates an electrical potential onto the transparent electrode, which is eventually used to recharge the internal battery. The perforation for acoustic transduction is created at the top of the TFFM, as depicted in the illustration **Figure 8(b)**. The TFFM transducer is produced using a straightforward method that involves placing a polymer mixture between two transparent electrodes. When acoustic vibrations occur, the flexible microphone device becomes activated, causing it to oscillate and generate a strong polarization (P). **Figure 8(c)** illustrates the schematic of a flexoelectric device that oscillates to generate sharp polarization. The mechanical drive of this electrical bending device is facilitated by the stress field (ε). In **Figure 8(d)**, a schematic representation of copolymer blending within a terpolymer matrix is displayed, resulting in a well-mixed chain structure of the copolymer and terpolymer molecules. **Figure 8(e)** presents a real photograph of the TFFM sensor. The relationship between its FLE effect, P, and mechanical stress is depicted in **Figure 8(f)**. Thanks to the increment of the zeta (z) phase, we report a FLE coefficient of $\mu = 23\ \mu C\ m^{-1}$ and a sensitivity of $S = 15\ V\ Pa^{-1}$, or 0.4 pC Pa^{-1}, for $\alpha = 0.5$ laminates at a frequency range of $10^1 \leq \omega\ (Hz) \leq 10^2$ at 10^2 dB SPL.

Experimental wavenumber (cm^{-1})	Vibration/group	Comments
3430	Symmetric stretching/N-H	—
3016	Symmetric stretching/CH2	—
2971	Asymmetric stretching/C-H	—
1453	In-plane bending or scissoring/CH2	—
1335 ± 2	In-plane bending or (wagging or twisting/ CH2-CF2	Zeta = α + ß (This Work)
840	CH2 Rocking and CF2 Asymmetric Stretching/ CH2/CF2	γ phase
763	In-plane bending or Rocking/CH2/CH2	α phase
745	In-plane bending or Rocking/CH2/CF2	ß phase
615	CF2 bending and CCC skeletal vibration/CH2/ CCC	α phase
500–1000	Bending/C-F	HH TT configuration
510	Bending and Wagging/CF2	ß phase
490	Bending and Wagging/CF2	α phase
445		ß phase

Table 2.
FTIR spectra for P(VDF) based (co/ter) polymers and its blends [61].

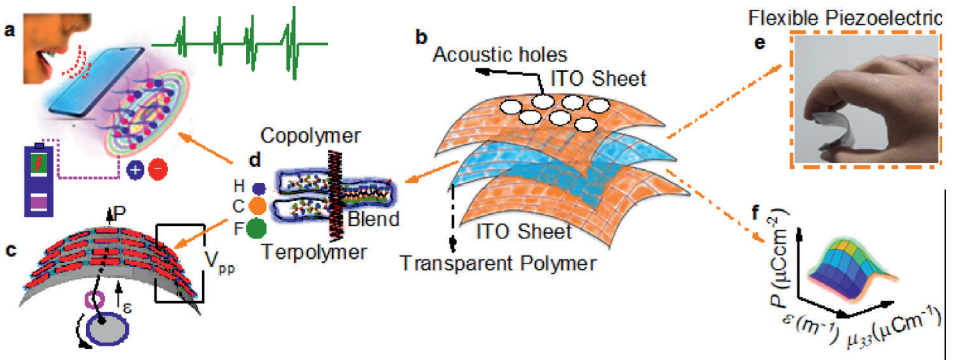

Figure 8.
The schematic diagram illustrates the TFFM microphone. (a) This diagram depicts a TFFM integrated into a mobile screen, capable of sensing and storing FLE energy to charge the smart device. (b) It displays the demonstration of piezoelectric laminates situated between two transparent electrodes, forming the TFFM transducers. (c) The schematic illustrates the ferroelectric (FE) effect of the piezoelectric transducer. (d) This part demonstrates the mixing of co and ter-polymer laminates. (e) A real-time photograph of the TFFM transducer is presented here. (f) The graphical representation outlines the mechanism of FE energy harvesting [61].

These values represent the highest recorded in the literature for the 70/30 P(VDF-TrFE) laminate, which previously had μ_{33} = 0.2μC m^{-1} and S = 10.9 V Pa^{-1} from 50 to 70 Hz.

Figure 9 illustrates the TFFM laminate created using blends ranging from 0 to 1 ($0 \leq \alpha \leq 1$). The schematic diagram of the transparent FE microphone laminate is shown in **Figure 9(a)**. **Figure 9(b)** presents an image of the actual microphone laminate fabricated in the lab. The transparency percentages of the transducers are depicted in **Figure 9(c)**, where the blends with α = 0.3 and α = 0.9 exhibit higher transparency compared to the other blends.

Piezoresponse Force Microscopy (PFM) images for blends with α = 0.1, 0.3, 0.5, and 1.0 are provided in **Figure 9(d)**. **Figure 9(e)** presents the piezoelectric coefficient behavior (d33 in pC/N) of the laminates, revealing that the d33 values for α = 0.5 and α = 0.7 are the highest. Additionally, **Figure 9(f)** details the FLE properties of the transparent microphone laminate, indicating that the α = 0.5 blend demonstrates greater ferroelectric properties than the other polymer blends.

A comparison of the FE coefficient (μ_{33}) across the blend system is illustrated in **Figure 9(g)**. The sensitivity of the laminates at various sound pressure levels is shown in **Figure 9(h–n)**, where the α = 0.5 blend exhibits the highest sensitivity among the tested blends. Consequently, we conducted real-time device tests on the α = 0.5 blend, with the results plotted in **Figure 9(o)**, demonstrating the microphone transducer's response to heart signals. Finally, **Figure 9(p)** displays the sound intensity (SI) as indicated by an oscilloscope for laminates ranging from α = 0 to 1, confirming that the sound intensity for α = 0.5 is greater than that of the other blend systems.

3.3 Piezo-capacitive two-in-one flexible transducer

In touch screen applications for smart devices, condenser transducers (CTs), also called piezo-capacitive transducers, have become essential. Unlike piezoresistive transducers, which detect shifts in impedance, CTs respond to variations in capacitance [64, 65]. A limitation of this technology is its need for a higher electric field to consistently achieve significant polarization (P) In PVDF-based condenser transducers, achieving significant polarization can require nearly hundreds of megavolts

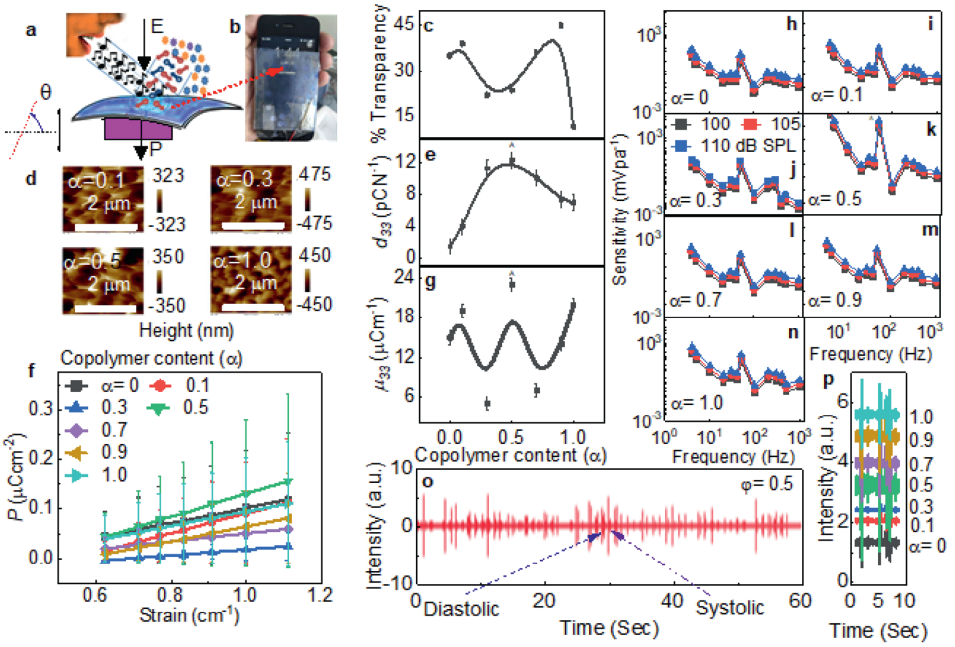

Figure 9.
Shows the TFFM laminate. (a) Depiction of FLE transducer laminate. (b) Photographs of lab-based laminates. (c) transparent (%) of laminates. (d)Piezoresponse Force Microscopic (PFM) photographs of blends. (e) Piezoelectric coefficient, d_{33} (pC/N) behavior of transducers. (f) FLE characteristics of transducers. (g) μ_{33} graphs of blends. (h-n) Sensitivity graphs at different SPL. (o) Real-time response of 50% (α = 0.5) transducer to check the actual heartbeat. (p) SI was checked by oscilloscope for various transducers (SD: n = 7) [61].

(around 100 MV/m). Recently, researchers have been focused on developing low-powered, flexible, and transparent transducer loudspeakers [66]. Consequently, recent literature reflects efforts to develop these transducers with reduced power consumption [60, 67]. Similarly, CTs utilize PVDF-based ferroelectric polymers also require high power to achieve optimal acoustic performance.

Currently, researchers are working to create low-power microphones tailored for potential smart device applications [68–70]. Modern smart societies require active machine/human interaction through smart household electronics applications. To facilitate this interaction, researchers are currently focusing on developing biomimetic multiresonant piezoelectric acoustic sensors (MRPEAS) [71–75] to improve the fidelity of CTs for total cochlear implants to enhance its at high electric field [76–78]. Recently, our group developed a TFPS transducer that achieves an enhanced sound pressure level (SPL) of 91 dB. We fabricated the laminates without insulating-paper material, which helped maintain their transparency [61].

Figure 10 Schematic diagrams of condenser transducers (CTs) include the following: on the left, a schematic representation of the Two-In-One (TIO) transducers, featuring the Condenser Microphone Unit (CMU); on the right, a schematic illustration of the Condenser Loudspeaker Unit (CLU).

CTs (i.e., CLU and CMU) are utilized to enhance fidelity, efficiency, and durability by incorporating suitable circuitry that compensates for their inherent properties. These CTs can function in either manner: as an input/output to an amplifier [80]. As a result, polymeric films have been engineered with embedded microstructures to enhance their acoustic properties, improving fidelity for voice recognition and recording applications

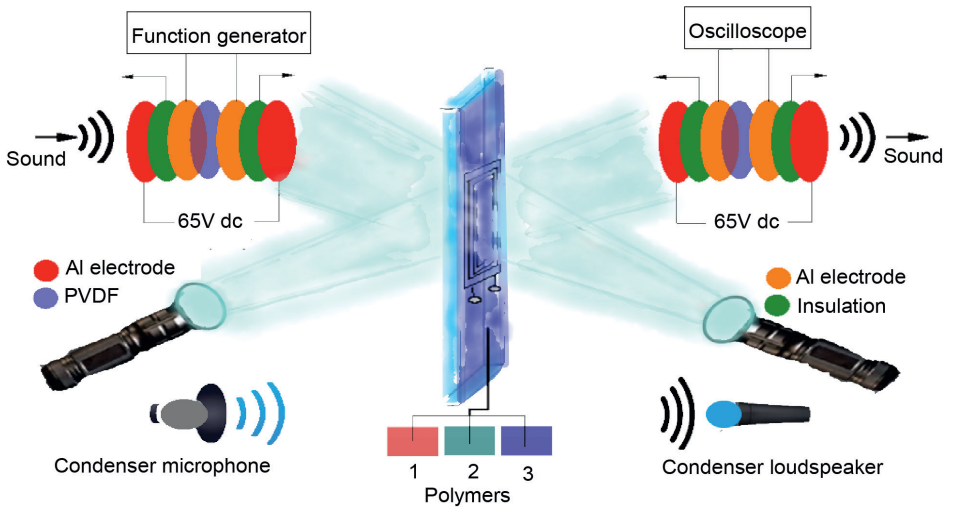

Figure 10.
Schematics of CTs [79].

[81]. The design and area of the active CTs are both crucial for achieving higher sound pressure levels (SPL) and optimal sound recognition. To address the challenges associated with larger area form factors, researchers have fabricated a diverse range of polymer film sensors, with results documented in recent reviews [82–86]. These designs enable the laminates to bend for enhanced performance efficiency; however, during bending, the layers become restricted, which ultimately reduces their acoustic performance [87].

Recently, a miniature condenser transducer (CT) featuring a silicon nitride membrane and a silicon backplate was developed for recording airborne sound. By simply stretching the diaphragm, the device achieved a sensitivity of approximately 1 V/Pa for sound signals ranging from −60 to −90 decibels (dB) [88]. Another transducer was reported that utilizes a silicon nitride diaphragm measuring 1.5 × 1.5 mm, along with a backplate. This design achieved a flat frequency response ranging from 10^2 Hertz to 10^1 kilohertz and a sensitivity of 0.19 mV/Pa with a bias voltage of approximately 65 V [89] fabricated using the sacrificial layer technique, a new Microelectromechanical Systems (MEMS) condenser transducer (CT) was developed featuring a porous diaphragm. By applying spin-on-glass (SOG) as a sacrificial electrode, this design achieved c.a. ~3 pF with a pull-in voltage of 1 megavolt.

Figure 11 shows the TIO CTs of blends. **Figure 11(a)** shows the SPL of blends at V = 0 and 65 V_{dc}. **Figure 11(b)** shows the temperature-dependent SPL (dB) which shows that the SPL is also dependent on the temperature. Also, **Figure 11(c)** provides information on the sound pressure level (SPL) and its associated noise across various frequencies. However, **Figure 11(d)** shows the polar graph of its noise at different frequency range. **Figure 11(e,f)** shows the square law graphs of blends at V = 0 and 65 V_{dc}. Consequently, **Figure 11(g)** shows the frequency visualization at V = 0 and 65 V_{dc} of polymer blends (Alpha, Beta, Gamma, Delta, and Exi) respectively.

This study presents the development of the TIO, CLU and CMU using a simple technique that sandwiches a PVDF laminate between a pair of two Al electrodes, each with a diameter of 3 cm^2. We achieved a sound pressure level (SPL) of 98 dB for the CLU at a capacitance of 0.51 nF for a Gamma blend with a voltage of 65 Vdc. The condenser unit demonstrated remarkable speech recognition capabilities, achieving a

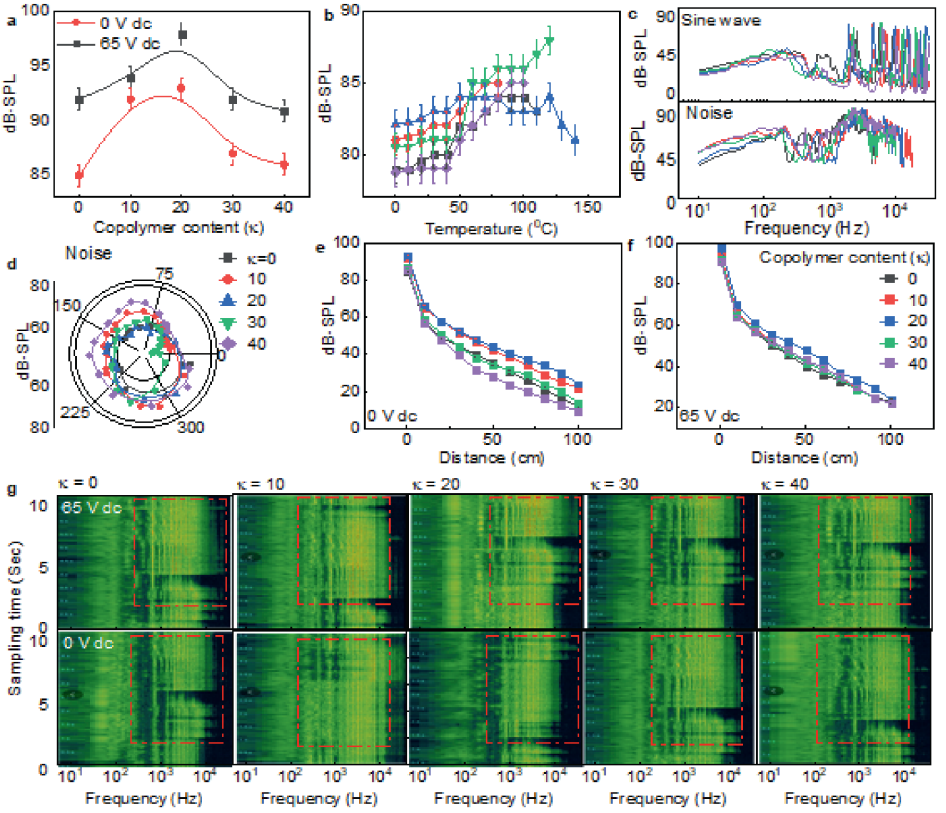

Figure 11.
CTs are made up of polymer blends. (a) SPL graph of blends at V = 0 and 65 V_{dc}. (b) Sound Pressure Level (SPL (dB)) Vs T graph. (c) SPL Vs noise at the graph. (d) Noise polar graph at variable frequencies (Hz). (e-f) Inverse graph of blends at V = 0 and 65 V_{dc}. (g) Frequency spectra graph (SD: n = 5) [79].

sensitivity of 0.9 V/Pa at approximately 10^0 Hz and 0.9 mV/Pa at 10^2 Hz for the Alpha blend. This resulted in clear speech recognition with minimal noise for both Alpha and Beta blends, exhibiting distinct frequency spectra due to their unique PE and AFE properties. In the TIO transducers, Beta CLU provided +5 dB-SPL sound efficiency, while the Beta CMU successfully recognized speech for sound signals ranging from 23.5 to 440 Hz at a voltage of 65 Vdc. The advancements in TIO, CLUs, and CMUs are poised to enhance smart devices by enabling simultaneous sound transmission and recording through a single transducer unit. **Figure 12** shows the information of CLUs and CMUs made up of blend system. **Figure 12(a)** shows the response of blends with respect to their voltage and operational frequency. **Figure 12(b)** represents the sensitivity of the sound intensity in which Gamma blend shows very good SI at 102 Hz. **Figure 12(c-d)** shows the sinewave graphs of the CT. **Figure 12(e)** represents the color visualization spectra of operational frequency for the blend system.

4. Conclusions

The electroactive properties of ferroelectric polymer blends were discussed, highlighting their advantages in terms of pyroelectric, piezoelectric, and

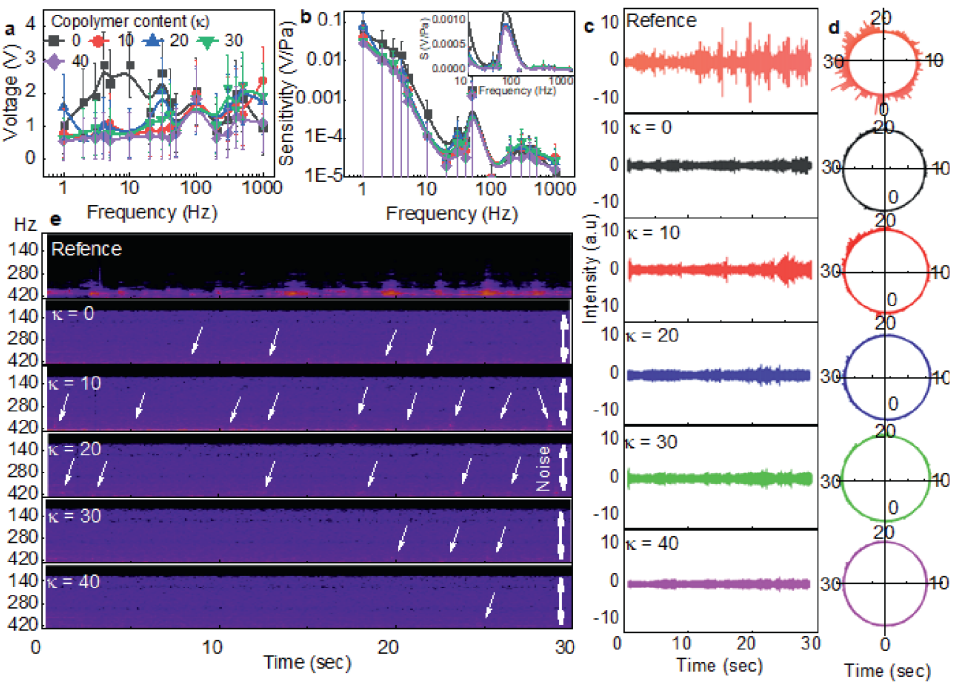

Figure 12.
CTs are fabricated by the polymer blend system. (a) Frequency (Hz) and Voltage trend. (b) Sound intensity (SI) plot. (c,d) Sinewave graphs of transducers. (e) Color visualization spectra of operational frequency for Alpha, Beta, Gamma, Delta, and Exi polymer blend systems (SD: n = 5) [79].

flexoelectric energy harvesting for flexible electronics. Well-known polymers, P(VDF-TrFE) and P(VDF-TrFE-CTFE) were mixed in a specific ratio, resulting in an antiferroelectric mixture through the creation of defect structures in the polymer blends. The antiferroelectric polymer blends were subjected to poling to enhance their beta phase, making them suitable for use as electroactive polymers in flexible electronics.

In this chapter, the pyroelectric, piezoelectric, and flexoelectric properties of the electroactive antiferroelectric polymer blend system are studied. It is reported that the electrostrictive properties of the blend system are enhanced (i.e., percentage of crystallinity enhanced from 10–70%, Energy Density is enhanced up to 1.44 J/cm^3 at near body temperature, the efficiency of Olsen cycle was increased by three fold, SPL is enhanced up to 91 dBSPL for flexible loudspeaker, sensitivity is enhanced by 10^3 mV/pa at 10^2 Hz in flexible microphone and SPL of TIO transducer was increased up to 96 dBSPL by applying the addition dc power source,) by increasing the copolymer content in the terpolymer matrix, which gradually increases its beta phase. This makes the material suitable for fabricating energy-harvesting devices and electroacoustic transducers for flexible electronics.

Acknowledgements

This work was supported by the National Natural Science Foundation of China (52072178).

Conflict of interest

There is no conflict of interest of all authors.

Notes/thanks/other declarations

We are thankful to Dr. Adeela Nasreen, Dr. Fahad Bin Zahid, and Dr., Zaighum Abbas Naqvi for their support in reviewing the document.

Author details

Mudassar Shehzad[1,2], Liu Yang[1] and Yaojin Wang[1*]

1 School of Materials Science and Engineering, Nanjing University of Science and Technology, Nanjing, China

2 Department of Materials Science and Engineering, Pak-Austria Fachhochschule: Institute of Applied Sciences and Technology, Haripur, Khyber Pakhtunkhwa, Pakistan

*Address all correspondence to: yjwang@njust.edu.cn

IntechOpen

© 2025 The Author(s). Licensee IntechOpen. This chapter is distributed under the terms of the Creative Commons Attribution License (http://creativecommons.org/licenses/by/4.0), which permits unrestricted use, distribution, and reproduction in any medium, provided the original work is properly cited. CC BY

References

[1] An N, Liu H, Ding Y, Zhang M, Tang Y. Preparation and electroactive properties of a PVDF/nano-TiO_2 composite film. Applied Surface Science. 2011;**257**:3831-3835. DOI: 10.1016/j.apsusc.2010.12.076

[2] Smith M, Kar-Narayan S. Piezoelectric polymers: Theory, challenges and opportunities. International Materials Reviews. 2022;**67**:65-88. DOI: 10.1080/09506608.2021.1915935

[3] Zhang QM, Bharti V, Zhao X. Giant electrostriction and relaxor ferroelectric behavior in electron-irradiated poly(vinylidene fluoride-trifluoroethylene) copolymer. Science. 1998;**280**:2101-2104. DOI: 10.1126/science.280.5372.2101

[4] Casar G, Li X, Koruza J, Zhang Q, Bobnar V. Electrical and thermal properties of vinylidene fluoride–trifluoroethylene-based polymer system with coexisting ferroelectric and relaxor states. Journal of Materials Science. 2013;**48**:7920-7926. DOI: 10.1007/s10853-013-7602-4

[5] Chu B, Zhou X, Ren K, Neese B, Lin M, Wang Q, et al. A dielectric polymer with high electric energy density and fast discharge speed. Science. 2006;**313**:334-336. DOI: 10.1126/science.1127798

[6] Guan F, Wang J, Yang L, Tseng J-K, Han K, Wang Q, et al. Confinement-induced high-field antiferroelectric-like behavior in a poly(vinylidene fluoride-co-trifluoroethylene-co-chlorotrifluoroethylene)-graft-polystyrene graft copolymer. Macromolecules. 2011;**44**:2190-2199. DOI: 10.1021/ma102910v

[7] Zhang Z, Meng Q, Chung TCM. Energy storage study of ferroelectric poly(vinylidene fluoride-trifluoroethylene-chlorotrifluoroethylene) terpolymers. Polymer. 2009;**50**:707-715. DOI: 10.1016/j.polymer.2008.11.005

[8] Su R, Tseng J-K, Lu M-S, Lin M, Fu Q, Zhu L. Ferroelectric behavior in the high temperature paraelectric phase in a poly(vinylidene fluoride-co-trifluoroethylene) random copolymer. Polymer. 2012;**53**:728-739. DOI: 10.1016/j.polymer.2012.01.001

[9] Bharti V, Hu H, Cheng ZY, Mai T, Zhang QM. Quantitative analysis of structural, relaxational and electrostrictive properties of PVDF-TRFE/PMMA films irradiated with high-energy electrons. IEEE Transactions on Dielectrics and Electrical Insulation. 2001;**8**:718-724. DOI: 10.1109/94.946729

[10] Chen X-Z, Li X, Qian X-S, Wu S, Lu S-G, Gu H-M, et al. A polymer blend approach to tailor the ferroelectric responses in P(VDF–TrFE) based copolymers. Polymer. 2013;**54**:2373-2381. DOI: 10.1016/j.polymer.2013.02.041

[11] Kittel C. Theory of antiferroelectric crystals. Physics Review. 1951;**82**:729-732. DOI: 10.1103/PhysRev.82.729

[12] Furukawa T, Takahashi Y, Nakajima T. Recent advances in ferroelectric polymer thin films for memory applications. Current Applied Physics. 2010;**10**:e62-e67. DOI: 10.1016/j.cap.2009.12.015

[13] Kong LB, Huang H, Li S. Fundamentals of ferroelectric materials. In: Ferroelectric Materials for Energy Applications. John

Wiley & Sons, Ltd; 2018. pp. 1-31. DOI: 10.1002/9783527807505.ch1

[14] Koizumi N, Murata Y, Tsunashima H. Polarization reversal and double hysteresis loop in copolymers of vinylidene fluoride and trifluoroethylene. IEEE Transactions on Electrical Insulation. 1986;**EI-21**:543-548. DOI: 10.1109/TEI.1986.348913

[15] Ducharme S, Reece TJ, Othon CM, Rannow RK. Ferroelectric polymer Langmuir-Blodgett films for nonvolatile memory applications. IEEE Transactions on Device and Materials Reliability. 2005;**5**:720-735. DOI: 10.1109/TDMR.2005.860818

[16] Gregorio R Jr. Determination of the α, β, and γ crystalline phases of poly(vinylidene fluoride) films prepared at different conditions. Journal of Applied Polymer Science. 2006;**100**:3272-3279. DOI: 10.1002/app.23137

[17] Yang L, Li X, Allahyarov E, Taylor PL, Zhang QM, Zhu L. Novel polymer ferroelectric behavior via crystal isomorphism and the nanoconfinement effect. Polymer. 2013;**54**:1709-1728. DOI: 10.1016/j.polymer.2013.01.035

[18] Silva JPB, Sekhar KC, Pan H, MacManus-Driscoll JL, Pereira M. Advances in dielectric thin films for energy storage applications, revealing the promise of group IV binary oxides. ACS Energy Letters. 2021;**6**:2208-2217. DOI: 10.1021/acsenergylett.1c00313

[19] Chang C, Tran VH, Wang J, Fuh Y-K, Lin L. Direct-write piezoelectric polymeric nanogenerator with high energy conversion efficiency. Nano Letters. 2010;**10**:726-731. DOI: 10.1021/nl9040719

[20] Mishra S, Unnikrishnan L, Nayak SK, Mohanty S. Advances in piezoelectric polymer composites for energy harvesting applications: A systematic review. Macromolecular Materials and Engineering. 2019;**304**:1800463. DOI: 10.1002/mame.201800463

[21] Kaval WG, Lake RA, Jr RAC. PVDF-TrFE electroactive polymer mechanical-to-electrical energy harvesting experimental bimorph structure. MRS Advances. 2017;**2**:3441-3446. DOI: 10.1557/adv.2017.397

[22] Wang D, Yuan G, Hao G, Wang Y. All-inorganic flexible piezoelectric energy harvester enabled by two-dimensional mica. Nano Energy. 2018;**43**:351-358. DOI: 10.1016/j.nanoen.2017.11.037

[23] Claude J, Lu Y, Li K, Wang Q. Electrical storage in poly(vinylidene fluoride) based ferroelectric polymers: Correlating polymer structure to electrical breakdown strength. Chemistry of Materials. 2008;**20**:2078-2080. DOI: 10.1021/cm800160r

[24] Wang Y, Luo C, Wang S, Chen C, Yuan G, Luo H, et al. Large piezoelectricity in ternary lead-free single crystals. Advanced Electronic Materials. 2020;**6**:1900949. DOI: 10.1002/aelm.201900949

[25] Campanini M, Trassin M, Ederer C, Erni R, Rossell MD. Buried in-plane ferroelectric domains in Fe-doped single-crystalline aurivillius thin films. ACS Applied Electronic Materials. 2019;**1**:1019-1028. DOI: 10.1021/acsaelm.9b00180

[26] Kawai H. The piezoelectricity of poly (vinylidene fluoride). Japanese Journal of Applied Physics. 1969;**8**:975. DOI: 10.1143/JJAP.8.975

[27] Furukawa T. Ferroelectric properties of vinylidene fluoride copolymers.

Phase Transitions. 1989;**18**:143-211. DOI: 10.1080/01411598908206863

[28] Sessler GM. Piezoelectricity in polyvinylidenefluoride. The Journal of the Acoustical Society of America. 1981;**70**:1596-1608. DOI: 10.1121/1.387225

[29] Eberle G, Schmidt H, Eisenmenger W. Piezoelectric polymer electrets. IEEE Transactions on Dielectrics and Electrical Insulation. 1996;**3**:624-646. DOI: 10.1109/94.544185

[30] Wang Y, Wen X, Jia Y, Huang M, Wang F, Zhang X, et al. Piezo-catalysis for nondestructive tooth whitening. Nature Communications. 2020;**11**:1328. DOI: 10.1038/s41467-020-15015-3

[31] Chen X, Luo L, Zeng Z, Jiao J, Shehzad M, Yuan G, et al. Bio-inspired flexible vibration visualization sensor based on piezo-electrochromic effect. Journal of Materiomics. 2020;**6**:643-650. DOI: 10.1016/j.jmat.2020.06.002

[32] Shehzad M, Malik T. Antiferroelectric behavior of P(VDF-TrFE) and P(VDF-TrFE-CTFE) ferroelectric domains for energy harvesting. ACS Applied Energy Materials. 2018;**1**:2832-2840. DOI: 10.1021/acsaem.8b00478

[33] Annapureddy V, Kim M, Palneedi H, Lee H-Y, Choi S-Y, Yoon W-H, et al. Low-loss piezoelectric single-crystal fibers for enhanced magnetic energy harvesting with magnetoelectric composite. Advanced Energy Materials. 2016;**6**:1601244. DOI: 10.1002/aenm.201601244

[34] Priya S, Song H-C, Zhou Y, Varghese R, Chopra A, Kim S-G, et al. A review on piezoelectric energy harvesting: Materials, methods, and circuits. Energy Harvesting and Systems. 2017;**4**:3-39. DOI: 10.1515/ehs-2016-0028

[35] Annapureddy V, Palneedi H, Hwang G-T, Peddigari M, Jeong D-Y, Yoon W-H, et al. Magnetic energy harvesting with magnetoelectrics: An emerging technology for self-powered autonomous systems. Sustainable Energy & Fuels. 2017;**1**:2039-2052. DOI: 10.1039/C7SE00403F

[36] Annapureddy V, Na S-M, Hwang G-T, Kang MG, Sriramdas R, Palneedi H, et al. Exceeding milli-watt powering magneto-mechano-electric generator for standalone-powered electronics. Energy & Environmental Science. 2018;**11**:818-829. DOI: 10.1039/C7EE03429F

[37] Park S, Kim Y, Jung H, Park J-Y, Lee N, Seo Y. Energy harvesting efficiency of piezoelectric polymer film with graphene and metal electrodes. Scientific Reports. 2017;**7**:1-8. DOI: 10.1038/s41598-017-17791-3

[38] Kishore RA, Priya S. A review on low-grade thermal energy harvesting: Materials. Methods and Devices, Materials. 2018;**11**:1433. DOI: 10.3390/ma11081433

[39] Ryu J, Kang J-E, Zhou Y, Choi S-Y, Yoon W-H, Park D-S, et al. Ubiquitous magneto-mechano-electric generator. Energy & Environmental Science. 2015;**8**:2402-2408. DOI: 10.1039/C5EE00414D

[40] Shehzad M, Wang Y. Structural tailing and pyroelectric energy harvesting of P (VDF-TrFE) and P (VDF-TrFE-CTFE) ferroelectric polymer blends. ACS Omega. 2020;**5**(23):13712-13718. DOI: 10.1021/acsomega.0c00871

[41] Hunter SR, Lavrik NV, Mostafa S, Rajic S, Datskos PG. Review of pyroelectric thermal energy harvesting and new MEMs-based resonant energy conversion techniques. In: Energy Harvesting and Storage: Materials,

Devices, and Applications III. SPIE; 2012. pp. 77-90. DOI: 10.1117/12.920978

[42] Goldsmid HJ. Principles of thermoelectric devices. British Journal of Applied Physics. 1960;**11**:209. DOI: 10.1088/0508-3443/11/6/301

[43] Lang SB. Pyroelectricity: From ancient curiosity to modern imaging tool. Physics Today. 2005;**58**:31-36

[44] Thakre A, Kumar A, Song H-C, Jeong D-Y, Ryu J. Pyroelectric energy conversion and its applications flexible energy harvesters and sensors. Sensors. 2019;**19**:2170. DOI: 10.3390/s19092170

[45] Chauhan A, Patel S, Vaish R, Bowen CR. Anti-ferroelectric ceramics for high energy density capacitors. Materials. 2015;**8**:8009-8031. DOI: 10.3390/ma8125439

[46] Fatuzzo E, Kiess H, Nitsche R. Theoretical efficiency of pyroelectric power converters. Journal of Applied Physics. 1966;**37**:510-516. DOI: 10.1063/1.1708205

[47] Chang D-A, Choh Y-H, Hsieh W-F, Lin P, Tseng T-Y. The role of drying-control chemical additives on the preparation of sol-gel derived PLZT thin films. Journal of Materials Science. 1993;**28**:6691-6698. DOI: 10.1007/BF00356416

[48] van der Ziel A. Solar power generation with the pyroelectric effect. Journal of Applied Physics. 1974;**45**:4128-4128. DOI: 10.1063/1.1663926

[49] Mohammed MS, Auner GW, Naik R, Mantese JV, Schubring NW, Micheli AL, et al. Temperature dependence of conventional and effective pyroelectric coefficients for compositionally graded BaxSr1−xTiO_3 films. Journal of Applied Physics. 1998;**84**:3322-3325. DOI: 10.1063/1.368516

[50] Lu SG, Rozic B, Kutnjak Z, Zhang QM, Lu SG, Rozic B, et al. Electrocaloric effect (ECE) in ferroelectric polymer films. In: Ferroelectrics. London, UK: IntechOpen; 2010. DOI: 10.5772/10483

[51] Wang TT, Herbert JM, Glass AM. The Applications of Ferroelectric Polymers. Blackie and Chapman and Hall; 1988. Available from: https://cir.nii.ac.jp/crid/1130282271181595904 [Accessed: October 6, 2024]

[52] Xia F, Cheng Z-Y, Xu HS, Li HF, Zhang QM, Kavarnos GJ, et al. High electromechanical responses in a poly(vinylidene fluoride–trifluoroethylene–chlorofluoroethylene) terpolymer. Advanced Materials. 2002;**14**:1574-1577. DOI: 10.1002/1521- 4095(20021104)14:21<1574::AID-ADMA1574>3.0.CO;2-#

[53] Tripathi AK, van Breemen AJJM, Shen J, Gao Q, Ivan MG, Reimann K, et al. Multilevel information storage in ferroelectric polymer memories. Advanced Materials. 2011;**23**:4146-4151. DOI: 10.1002/adma.201101511

[54] Kasap S. Principles of Electronic Materials and Devices. 3rd ed. USA: McGraw-Hill, Inc.; 2005

[55] Shehzad M, Ahmed S, Siddiqui F, Bukhari SZA, Zahid FB, Akram F, et al. Frequency-dependent ferroelectric heat cycles in polymer blends: Enhancements in electrocaloric performance of P(VDF-TrFE) and P(VDF-TrFE-CTFE). Polymer. 2025;**316**:127881. DOI: 10.1016/j.polymer.2024.127881, ISSN 0032-3861

[56] Borwick J. Loudspeaker and Headphone Handbook. Focal Press; n.d.. Available from: https://sc.panda985.com/extdomains/books.google.com/books/about/Loudspeaker_and_

Headphone_Handbook.html?hl=zh-CN&id=TscrBgAAQBAJ [Accessed October 6, 2024]

[57] Newell P, Holland K. Loudspeakers: For Music Recording and Reproduction. 2nd ed. New York: Routledge; 2018. DOI: 10.4324/9781315149202

[58] Wang Y-T, Hu Y-C, Chen K-R. A flexible polyvinylidene fluoride film-loudspeaker. 中國機械工程學刊. 2015;**36**:59-66

[59] White DR. Wide-range electrostatic loudspeaker with a zero-free polar response. Journal of the Audio Engineering Society. 2009;**57**:822-831

[60] Ohga J. A flat piezoelectric polymer film loudspeaker as a multi-resonance system. Journal of the Acoustical Society of Japan (E). 1983;**4**:113-120. DOI: 10.1250/ast.4.113

[61] Shehzad M, Wang S, Wang Y. Flexible and transparent piezoelectric loudspeaker. Npj Flexible Electronics. 2021;**5**:1-6. DOI: 10.1038/s41528-021-00121-z

[62] Lee CS, Kim JY, Lee DE, Joo J, Wagh BG, Han S, et al. Flexible and transparent organic film speaker by using highly conducting PEDOT/PSS as electrode. Synthetic Metals. 2003;**139**:457-461. DOI: 10.1016/S0379-6779(03)00199-1

[63] Sugimoto T, Ono K, Ando A, Kurozumi K, Hara A, Morita Y, et al. PVDF-driven flexible and transparent loudspeaker. Applied Acoustics. 2009;**70**:1021-1028. DOI: 10.1016/j.apacoust.2009.03.007

[64] Weigold JW, Brosnihan TJ, Bergeron J, Zhang X. A MEMS condenser microphone for consumer applications. In: 19th IEEE International Conference on Micro Electro Mechanical Systems. 2006. pp. 86-89. DOI: 10.1109/MEMSYS.2006.1627742

[65] Zhang Z, Wang L, Lee C. Recent advances in artificial intelligence sensors. Advanced Sensor Research. 2023;**2**:2200072. DOI: 10.1002/adsr.202200072

[66] Xu SC, Man BY, Jiang SZ, Chen CS, Yang C, Liu M, et al. Flexible and transparent graphene-based loudspeakers. Applied Physics Letters. 2013;**102**:151902. DOI: 10.1063/1.4802079

[67] Piezoelectricity. n.d. Available from: https://sc.panda985.com/extdomains/books.google.com/books/about/Piezoelectricity.html?hl=zh-CN&id=8KyawZ92eIEC [Accessed October 6, 2024]

[68] Park S, Guan X, Kim Y, Creighton FXP, Wei E, Kymissis I, et al. PVDF-based piezoelectric microphone for sound detection inside the cochlea: Toward totally implantable cochlear implants. Trends in Hearing. 2018;**22**:2331216518774450. DOI: 10.1177/2331216518774450

[69] Åkerfeldt M, Lund A, Walkenström P. Textile sensing glove with piezoelectric PVDF fibers and printed electrodes of PEDOT: PSS. Textile Research Journal. 2015;**85**(17):1789-1799. DOI: 10.1177/0040517515578333

[70] Choi S, Jiang Z. A novel wearable sensor device with conductive fabric and PVDF film for monitoring cardiorespiratory signals. Sensors and Actuators A: Physical. 2006;**128**:317-326. DOI: 10.1016/j.sna.2006.02.012

[71] Jung YH, Hong SK, Wang HS, Han JH, Pham TX, Park H, et al. Flexible

piezoelectric acoustic sensors and machine learning for speech processing. Advanced Materials. 2020;**32**:1904020. DOI: 10.1002/adma.201904020

[72] Shintaku H, Nakagawa T, Kitagawa D, Tanujaya H, Kawano S, Ito J. Development of piezoelectric acoustic sensor with frequency selectivity for artificial cochlea. Sensors and Actuators A: Physical. 2010;**158**:183-192. DOI: 10.1016/j.sna.2009.12.021

[73] Lee HS, Chung J, Hwang G-T, Jeong CK, Jung Y, Kwak J-H, et al. Flexible inorganic piezoelectric acoustic nanosensors for biomimetic artificial hair cells. Advanced Functional Materials. 2014;**24**:6914-6921. DOI: 10.1002/adfm.201402270

[74] Lang C, Fang J, Shao H, Ding X, Lin T. High-sensitivity acoustic sensors from nanofibre webs. Nature Communications. 2016;**7**:11108. DOI: 10.1038/ncomms11108

[75] Jang J, Lee J, Woo S, Sly DJ, Campbell LJ, Cho J-H, et al. A microelectromechanical system artificial basilar membrane based on a piezoelectric cantilever array and its characterization using an animal model. Scientific Reports. 2015;**5**:1-13. DOI: 10.1038/srep12447

[76] Je CH, Lee J, Yang WS, Kim J, Cho Y-H. A surface-micromachined capacitive microphone with improved sensitivity. Journal of Micromechanics and Microengineering. 2013;**23**:055018. DOI: 10.1088/0960-1317/23/5/055018

[77] Walser S, Siegel C, Winter M, Feiertag G, Loibl M, Leidl A. MEMS microphones with narrow sensitivity distribution. Sensors and Actuators A: Physical. 2016;**247**:663-670. DOI: 10.1016/j.sna.2016.04.051

[78] Ali WR, Prasad M. Piezoelectric MEMS based acoustic sensors: A review. Sensors and Actuators A: Physical. 2020;**301**:111756. DOI: 10.1016/j.sna.2019.111756

[79] Shehzad M, Wang Y. PVDF based piezoelectric condenser loudspeaker and microphone. Sensors and Actuators A: Physical. 2022;**346**:113861. DOI: 10.1016/j.sna.2022.113861

[80] Edelman PE. Condenser loudspeaker with flexible electrodes. Proceedings of the Institute of Radio Engineers. 1931;**19**:256-267. DOI: 10.1109/JRPROC.1931.222311

[81] Miao H, Li C, Wang J. A future of smarter digital health empowered by generative pretrained transformer. Journal of Medical Internet Research. 2023;**25**:e49963. DOI: 10.2196/49963

[82] Dias T, Monaragala R, Soleimani M. Acoustic response of a curved active PVDF-paper/fabric speaker for active noise control of automotive interior noise. Measurement Science and Technology. 2007;**18**:1521. DOI: 10.1088/0957-0233/18/5/043

[83] Guigou C, Fuller CR. Control of aircraft interior broadband noise with foam-PVDF SMART skin. Journal of Sound and Vibration. 1999;**220**:541-557. DOI: 10.1006/jsvi.1998.1972

[84] Han JH, Bae KM, Hong SK, Park H, Kwak J-H, Wang HS, et al. Machine learning-based self-powered acoustic sensor for speaker recognition. Nano Energy. 2018;**53**:658-665. DOI: 10.1016/j.nanoen.2018.09.030

[85] Elfes A. Sonar-based real-world mapping and navigation. IEEE Journal on Robotics and Automation. 1987;**3**:249-265. DOI: 10.1109/JRA.1987.1087096

[86] Wells PNT. Ultrasonic imaging of the human body. Reports on Progress in Physics. 1999;**62**:671. DOI: 10.1088/0034-4885/62/5/201

[87] Hohm D, Hess G. A subminiature condenser microphone with silicon nitride membrane and silicon back plate. The Journal of the Acoustical Society of America. 1989;**85**:476-480. DOI: 10.1121/1.397699

[88] Scheeper PR, Olthuis W, Bergveld P. A silicon condenser microphone with a silicon nitride diaphragm and backplate. Journal of Micromechanics and Microengineering. 1992;**2**:187. DOI: 10.1088/0960-1317/2/3/016

[89] Ganji BA, Nateri MS, Dardel M. Design and modeling of a novel high sensitive MEMS piezoelectric vector hydrophone. Microsystem Technologies. 2018;**24**:2085-2095. DOI: 10.1007/s00542-018-3770-0